OPEN

Scalable Functionalized Graphene Nano-platelets as Tunable Cathodes for High-performance Lithium Rechargeable Batteries

Haegyeom Kim[1], Hee-Dae Lim[1], Sung-Wook Kim[1], Jihyun Hong[1], Dong-Hwa Seo[1], Dae-chul Kim[2], Seokwoo Jeon[2], Sungjin Park[3] & Kisuk Kang[1]

[1]Department of Materials Science and Engineering, Research Institute of Advanced Materials, Seoul National University, Gwanak-ro, Gwanak-gu, Seoul 151-742 (Republic of Korea), [2]Department of Materials Science and Engineering, KAIST, 291 Daehak-ro, Yuseong-gu, Daejeon 305-701 (Republic of Korea), [3]Department of Chemistry, Inha University, 100 Inharo, Nam-gu, Incheon 402-751 (Republic of Korea).

High-performance and cost-effective rechargeable batteries are key to the success of electric vehicles and large-scale energy storage systems. Extensive research has focused on the development of (i) new high-energy electrodes that can store more lithium or (ii) high-power nano-structured electrodes hybridized with carbonaceous materials. However, the current status of lithium batteries based on redox reactions of heavy transition metals still remains far below the demands required for the proposed applications. Herein, we present a novel approach using tunable functional groups on graphene nano-platelets as redox centers. The electrode can deliver high capacity of ~250 mAh g^{-1}, power of ~20 kW kg^{-1} in an acceptable cathode voltage range, and provide excellent cyclability up to thousands of repeated charge/discharge cycles. The simple, mass-scalable synthetic route for the functionalized graphene nano-platelets proposed in this work suggests that the graphene cathode can be a promising new class of electrode.

The development of electrode materials that combine high energy and power density with low cost is an ongoing challenge for energy storage[1]. Current lithium ion batteries (LIBs) use intercalation compounds that contain transition metals for positive electrode materials. While the high redox potential of transition metals in the electrode materials contributes to the high voltage of LIBs, the presence of heavy transition metals increases the molecular weight, thus substantially decreasing the capacity. For example, about 60% of the molecular weight of LiCoO$_2$ (mw = 97.874 g mol^{-1}), the most widely used cathode, comes from Co (mw = 58.933 g mol^{-1}), and transition metals constitute a major portion of the material cost[2–4]. Furthermore, some transition metals that are commonly used for redox reactions in cathodes are not environmentally benign.

Current electrode chemistry based on intercalation does not supply sufficient power density for LIBs applications because (i) relatively slow solid-state lithium diffusion should take place during intercalation and (ii) the electrical conductivity of such compounds is often semi-conducting or even insulating[5–7]. This has, in turn, given rise to rigorous research on the synthesis of nanostructured electrodes hybridized with conductive carbonaceous materials[8–25]. However, the synthesis of nanostructured electrodes is not trivial and often induces structural defects, which are detrimental to Li diffusion during intercalation. Also, the additional weight from the conductive agent decreases the energy density per total electrode weight.

A promising resolution to both energy and power density limitations is the use of a transition-metal-free conductive agent, itself, as an active material with a non-intercalation-based lithium storage reaction[26–31]. In this paper, we propose new type of electrode materials for LIBs using functionalized graphene nano-platelets with tunable power and energy density. It is noted that the previous research on graphene electrodes has been focused primarily on anode applications[32,33]. The electrochemical reaction mechanisms and redox potentials of anode and cathode are certainly different and it is generally accepted that the discovery of cathode material is more challenging because the hosting material should store lithium with much higher potential (*e.g.* much lower lithium chemical potential). Only certain chemistries allow the lithium to be stored in the host with potentials

1

suitable for cathode. This work manipulating graphene from conventional anode activity to cathode region will point at an interesting new direction for electrode materials development.

The simple and cost-effective process suggested here could produce graphene nano-platelets with programmed functionalities in a porous microstructure. The fast surface Faradaic reactions of functional groups in graphene nano-platelets, combined with high electrical conductivity and porous morphology, could significantly increase energy and power density. The functionalized graphene nano-platelets delivered high energy ($\sim$260 Wh $kg_{electrode}^{-1}$) at an exceptionally high power ($\sim$20 kW $kg_{electrode}^{-1}$) without noticeable capacity fading after thousands of battery cycles (2,000 cycles). The energy density of the nano-platelets was much higher than that of conventional high-power LIB electrodes ($\sim$6 kW $kg_{electrode}^{-1}$)[34]. Furthermore, we demonstrated that the surface reaction between functional groups and lithium ions can be tuned by controlling the functionalities of graphene nano-platelets so that the electrochemical performance, including energy and power density, can be optimized. The simple and mass-scalable chemical method for synthesizing functionalized graphene nano-platelets used in this work will be beneficial for the economy and for commercialization.

Results

One-step fabrication of functionalized graphene nano-platelets with a porous structure. Functionalized graphene nano-platelets were synthesized by controlled oxidation of pristine graphite and subsequent one-step low-temperature ($\sim$120°C) annealing. To obtain samples with different amounts of functional groups,

graphite was oxidized while adjusting the amount of oxidizing agent. Our primary focus was to partly reduce the graphite oxide (GO) and obtain a porous microstructure using a simple process. An optimal porous microstructure was expected to facilitate the efficient transport of lithium ions from the electrolyte through the micropores during fast charge and discharge. In our one-step partial reduction process, we found that the solvent molecules, which were trapped in the interlayer galleries of hydrophilic GO during the washing step, played an important role in the generation of a porous structure upon annealing at 120°C. Various solvents were considered to optimize the porous morphology of the functionalized graphene nano-platelets from HBr to NH_3 with different vapor pressure, as shown in Figure 1a[35] (order of increasing vapor pressure: NH_3 > HCl > DI, H_2SO_4, CH_3COOH, HNO_3, HBr). Figure 1 shows that pristine graphite (Figure 1b) was oxidized to GO (Figure 1c) with interlayer expansion. During annealing at 120°C, the GO (washed in deionized (DI) water), showed mild exfoliation with visible pores along the graphene nano-platelets (Figure 1d). Previous reports have described similar behavior; pore formation was attributed to the sudden evaporation of water molecules trapped between the GO layers and to gas generation by thermal decomposition of labile oxygen functionalities[36–38]. Inspired by this, we decided to use solutions with higher vapor pressures than water to enhance the effect. GO washed with an additional HCl solution (37 wt%) was annealed (Figure 1e), resulting in uniform pores with sizes ranging from a few tens to a few hundred nanometers; the 10-nm-thick graphene nano-platelets covered a large area, with simultaneous partial reduction. The pore formation by the gas evolution implies
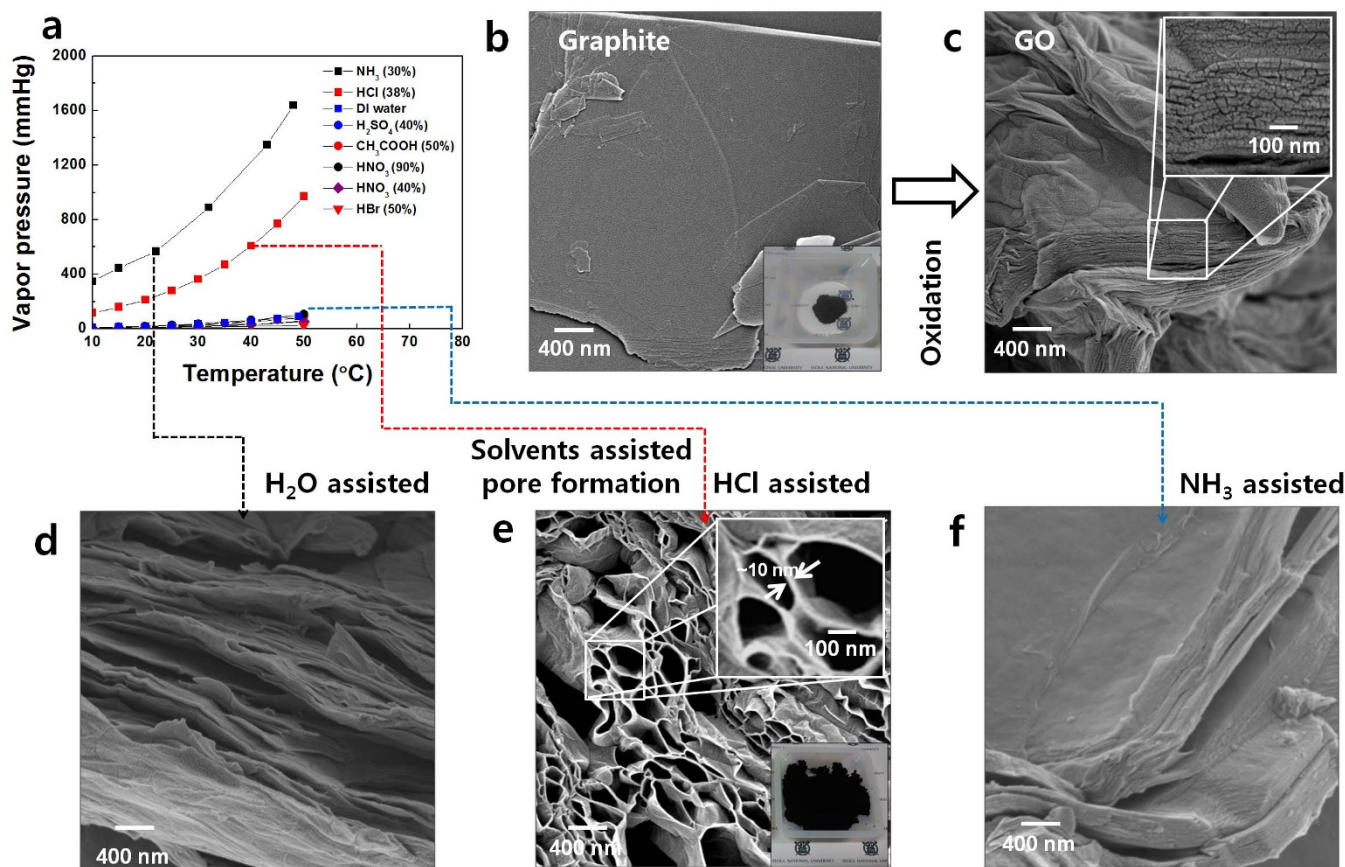

Figure 1 | Solvent-assisted pore formation of the functionalized graphene nano-platelets. (a) Vapor pressures of various solvents (NH_3, HCl, water, H_2SO_4, CH_3COOH, HNO_3, HBr) from 10 to 50°C, obtained from literature data (Ref. 35). (b) FE-SEM images of pristine graphite (inset: photo of pristine graphite). (c) GO oxidized from pristine graphite. FE-SEM images of GO samples that were assisted by (d) H_2O, (e) HCl (inset: photo of HCl-assisted sample after annealing), and (f) NH_3. NH_3- and H_2O-assisted samples do not show porous morphology; the HCl-assisted sample had pores (a few hundred nanometers in diameter).

that the pores are interconnected from the inside to the surface of the material. We believe this pore formation mechanism is advantageous in that facile accessibility of the electrolyte is also possible[39,40]. The gas evolution path which interconnects the inside and the surface of the material is expected to provide the efficient transport route for lithium ions in the electrolyte through the micropores during fast charge and discharge. From the laser scanning confocal microscopic analysis in Figure S1, we could have a glance at the micropores that are connected throughout the graphene cathode. Evidence of the partial reduction of GO is provided in the following paragraph. We believe that the HCl solution trapped in the interlayer galleries of GO exhibited stronger exfoliation than HCl-free water when heated to 120°C because the vapor pressure of the HCl solution was higher than that of water. The bottom inset in Figure 1e shows a photograph of the resultant sample, indicating a large expansion of the powder volume compared to the pristine graphite (inset in Figure 1b). In order to confirm the pore generation was mainly affected by the vapor pressure, it was examined whether acidic media catalyze GO's thermal decomposition or not. However, other acidic media such as CH_3COOH and H_2SO_4 did not show any notable catalytic effects on generating pores (Figure S2). The use of a solution with even higher vapor pressure, NH_3 solution

(30 wt%), however, did not exfoliate the GO (Figure 1f). This was probably because the NH_3 molecules could be easily evaporated from the sample before reaching the boiling temperature of the NH_3 solution. Finally, the scalability of the process was examined by preparing a large quantity of functionalized graphene nano-platelet samples with 30 gram scales as shown in Figure S3. By proportionally increasing the amount of precursor materials, the fabrication was easily scalable with a high yield about 95%. X-ray photoelectron spectroscopy (XPS) and X-ray diffraction (XRD) analysis of the functionalized graphene nano-platelets revealed that the GO was reduced by low-temperature annealing. The XRD pattern in Figure 2a (above) shows that the main GO peak shifted from 10° to 24° and broadened because of the reduction of GO and the loss of long-range ordering of graphene planes[16,41]. The bottom of Figure 2a compares the sample before and after annealing. The presence of two distinct peaks (286.6 and 287.6 eV) in the C 1s spectrum was attributed to carbon atoms in C–O moieties on the basal planes of nano-platelets and C=O moieties at the edges of nano-platelets[42–44]. Both C–O and C=O bonds in GO were significantly reduced after annealing. Fourier transform infrared (FT-IR) spectroscopy (Figure S4) further identified the partial reduction of GO. Simultaneous reduction and exfoliation during low-temperature annealing was
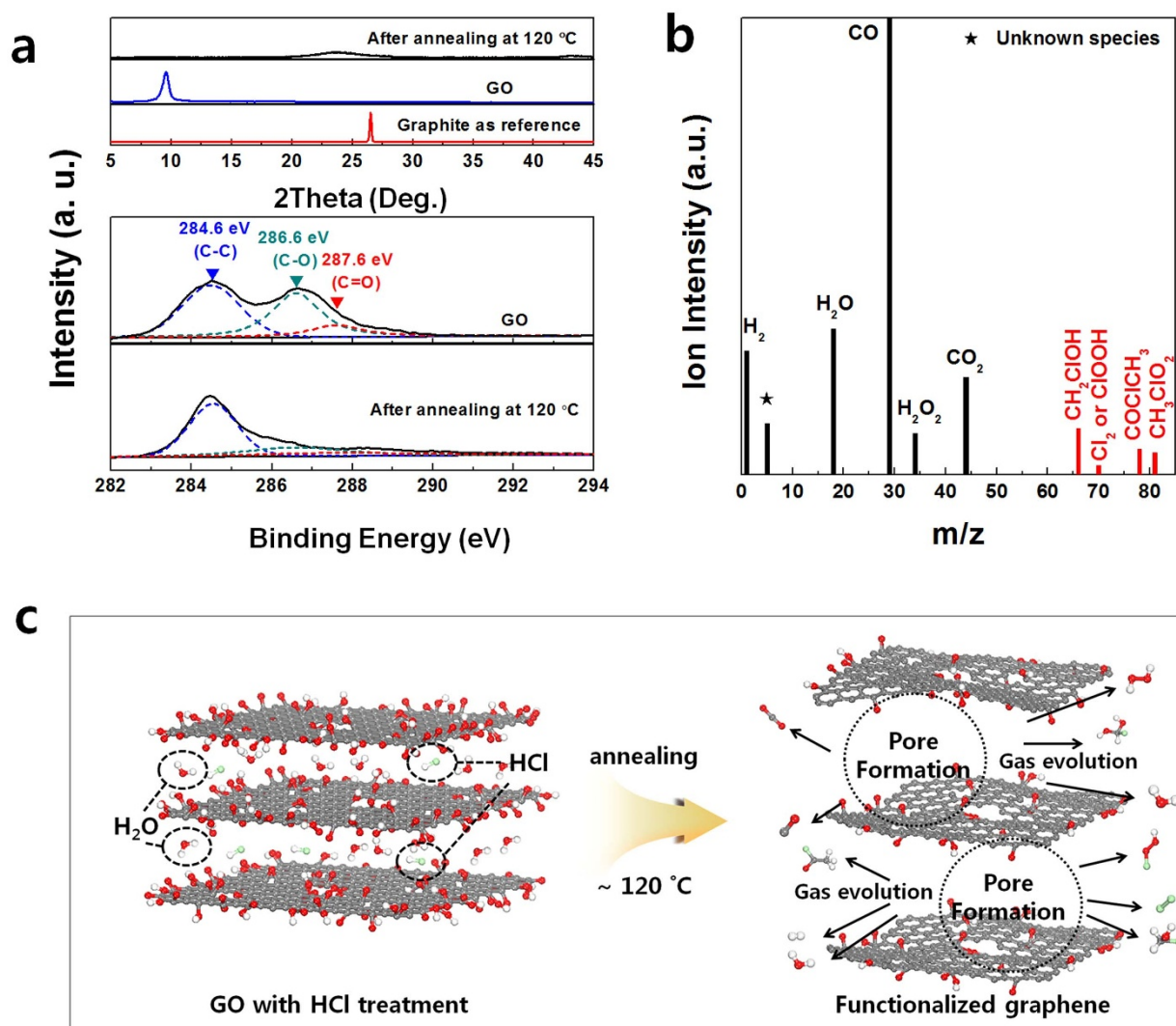

Figure 2 | Pore formation and reduction mechanism. (a) XRD (above) and XPS (bottom) analysis results for GO and functionalized graphene nano-platelets after annealing at 120°C. (b) MS analysis result of gases that evolved after HCl-treated GO sample were heated at 120°C. Gas species with high molecular weights were thought to be Cl-containing molecules such as CH_2ClOH, $ClOOH$, $CCOClCH_3$, and CH_3ClO_2, which explains the reduction effects of HCl on GO. (c) Schematic drawing of the pore formation and reduction mechanism.

monitored with *ex-situ* and *in-situ* mass spectrometry (MS), as shown in Figure 2b and Figure S5. Gas evolution of CO, H_2O, H_2, CO_2, and H_2O_2 resulted from reactions between functional groups and carbon atoms in GO[45,46]. Gas evolution occurred in a relatively short time, as shown in the *in-situ* MS results in Figure S5, which may explain the exfoliation at this temperature. The detection of gas species with molecular weights greater than 60 was attributed to the reaction of HCl with functional groups. The formation of Cl-containing molecules, such as CH_2ClOH, $ClOOH$, $CCOClCH_3$, and CH_3ClO_2, indicates additional reduction effects of HCl. The reduction effects of HCl were further identified by XPS analysis (Figure S6). HCl-washed samples contained significantly fewer functional groups than water-washed and NH_3-washed samples, suggesting that the introduction of HCl treatment enhanced the reduction of GO at 120°C more effectively than water or even NH_3 which is known to reduce GO.

The schematic illustration in Figure 2c shows the proposed mechanism of pore formation and reduction when GO is heated to 120°C after HCl treatment. During HCl treatment, HCl and H_2O molecules are intercalated into the interlayer galleries of hydrophilic GO. As a result of dramatically increased vapor pressure in the presence of HCl upon heating, simultaneous exfoliation and pore formation occur. During gas evaporation, the paths of escaping gases create interconnected micropores within the sample. It is worthwhile to note that the connectivity of pores is important in facile lithium transport within the electrode during battery operation.

Control of the graphene nano-platelet functionality. Samples containing different amounts of functional groups were prepared by adjusting the amount of oxidizing agent in preparing GO but using the same one-step low-temperature reduction. Four samples with different target amounts of functional groups are denoted as HFG (high-content functional group), MFG (medium-content functional group), LFG (low-content functional group), and MFG-400, which denotes the MFG sample with an additional thermal reduction at 400°C. The label of HFG, MFG, and LFG were based on the content of functional groups, especially, C=O group. It should be noted that the sample in the previous section was MFG, and the porous morphology of all the samples were identical regardless of the amount of functional groups (Figure S7). XPS analysis revealed that the amount of residual functional groups could be systematically controlled by modifying the oxidation processes proposed in this work (Figure 3a). The peaks from C–O and C=O bonding in the C1s XPS spectra correspond well with the targeted degree of functionalization of the samples. HFG contained the highest content of C–O and C=O, while MFG-400 contained the lowest content of C–O and C=O bonds.
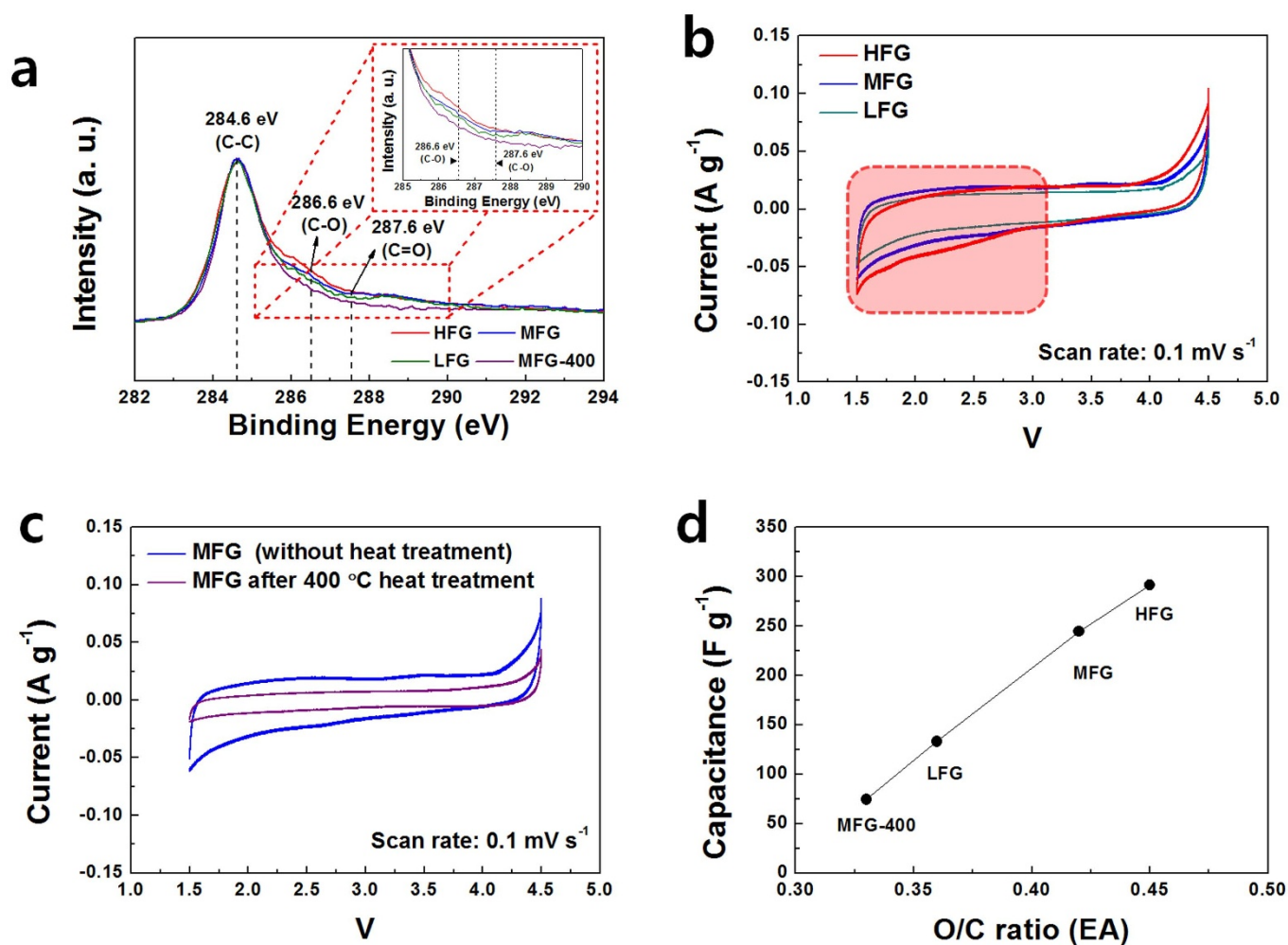

Figure 3 | Functionality-dependant electrochemical behavior of the functionalized graphene nano-platelets. (a) XPS C 1s spectra of the functionalized graphene nano-platelets with different degrees of oxidation. (b) CV data for the functionalized graphene nano-platelet samples over a voltage range from 1.5 to 4.5 V with a scan rate of 0.1 mV s⁻¹. (c) CV data for the functionalized graphene nano-platelets with and without heat treatment at 400°C under an Ar atmosphere for 6 h. (d) Relationship between the O/C ratio and gravimetric capacitance, which indicates that the gravimetric capacitance increased linearly with the O/C ratio of the functionalized graphene nano-platelets.
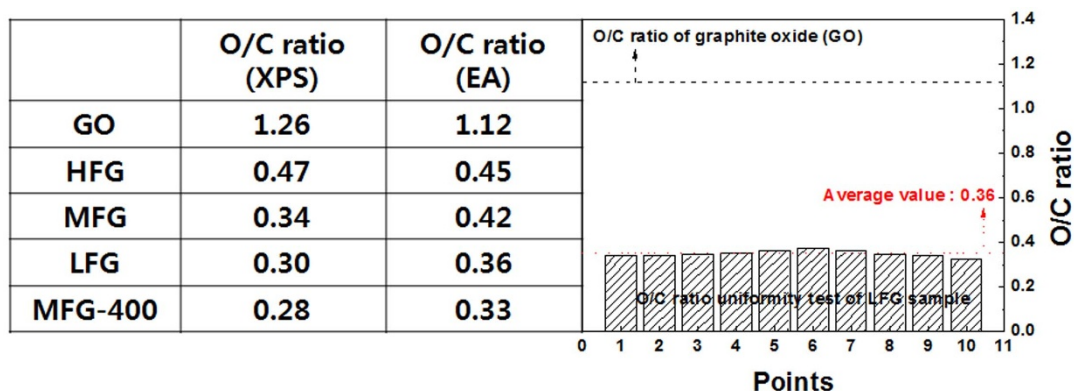
4

Figure 4 | O/C ratio analysis of the functionalized graphene nano-platelets and O/C ratio uniformity. O/C ratio analysis data obtained from XPS and EA (left table). (The differences in the O/C ratios for XPS and EA results were related to the analysis conditions, *i.e.*, vacuum and ambient air atmospheres. The trend in the O/C ratio for the two techniques was consistent.) The O/C ratio uniformity of the LFG sample was tested using the EA (right figure). Ten points were randomly collected from the LFG sample. The O/C ratio shows only a small variation from the average value of 0.36.

The atomic composition of each sample was further analyzed with an element analyzer (EA) and tabulated in Figure 4 along with the values obtained from XPS analysis. The O/C ratio is about 1.12 for GO, and was reduced to 0.45 for HFG and 0.33 for MFG-400. The different O/C ratios obtained by XPS and EA analysis may be due to the experimental conditions of the analysis, *i.e.*, vacuum (XPS) and ambient air (EA) atmospheres, but the overall trend of the O/C ratio was consistent. Because the reduction occurred rapidly, the uniformity of the O/C ratio within a sample was also carefully investigated. We randomly chose 10 points in the LFG sample and analyzed the O/C ratio. The O/C ratios at the 10 points were similar, as shown in F (right), which indicated that the O/C ratio was uniform throughout the sample, despite the rapid reduction process.

Functionality-dependent electrochemical behavior. Cyclic voltammetry (CV) data of the functionalized graphene nano-platelets demonstrated that surface Faradaic reactions were responsible for the electrochemical reactivity (Figure 3b). CV measurements of the samples were conducted in the voltage range of 1.5 to 4.5 V with 0.1 mV s^{-1} scan rate. Gravimetric capacitance was increased from 133.2 F g^{-1} (LFG sample) to 291.6 F g^{-1} (HFG sample), which coincided with the degree of oxidation of each sample. Increased capacitance was mainly observed over a voltage range from 3.0 to 1.5 V, as illustrated in the shaded region of Figure 3b. Recently, it was reported that carbonyl (C=O) groups can be reversibly reduced and oxidized with Li ions over a voltage range from 3.5 to 1.5 V in aromatic carbonyl derivative organic materials such as Li$_2$C$_6$O$_6$[47], 3, 4, 9, 10-perylene-tetracarboxylicacid-dianhydride sulfide polymer[48], and poly (2,5-dihydoxy-1,4-benzoquinon-3,6-methylene)[49]. Higher gravimetric capacitance due to the higher degree of oxidation was attributed to an increase in Faradaic reactions of surface functional groups on the functionalized graphene nano-platelets.

The specific capacitance values of the functionalized graphene nano-platelets (MFG sample) before and after heat treatment were compared to further confirm the role of functional groups in providing high capacitance. Functional groups on the MFG were further removed with heat treatment at 400°C without changing the morphology of graphene nano-platelets (Figure S7). Gravimetric current and capacitance values were decreased by a factor of ~0.3 after heat treatment (Figure 3c). As shown in Figure 3a and Figure 4, heat treatment decreased the O/C ratio; thus, this experiment strongly suggests that the Faradaic reactions of functional groups with lithium ions are responsible for the large gravimetric capacitance of the functionalized graphene nano-platelets. Additionally, the linear relationship between the O/C ratio and gravimetric capacitance (Figure 3d) provides further evidence that the redox reactions of

oxygen-containing functional groups with lithium ions primarily contributed to the high gravimetric capacitances.

Functionalized graphene nano-platelets as cathodes in lithium ion batteries. The dependence of lithium storage capability on functionality was identified by potentio-galvanostat tests. Figure 5a shows that the specific capacity of the functionalized graphene nano-platelets increased according to the amount of functional groups. The specific capacities were ~239, 178, and 150 mAh g^{-1} for HFG, MFG, and LFG, respectively, at a current density of ~100 mA g^{-1}. The charge/discharge profiles of each sample were identical, indicating that they undergo an identical electrochemical reaction. The linear increase in specific capacity with increasing functional groups supports the proposed redox reaction mechanism between functional groups and lithium. To identify the redox center for lithium storage, *ex-situ* XPS and *ex-situ* FT-IR analysis were used (Figure 5b, 5c, and Figure S8). It was found that the lithium ions are stored *via* the reaction with the C=O functional groups. Figure 5b reveals that the lithium ions were stored in in the discharged state. Correspondingly, XPS peak from C=O functional group was reduced and that from C–O functional group was substantially increased in Figure 5c. This indicates the lithium ions were stored at C=O functional groups by breaking the double bonds and forming the single bonds between carbon and oxygen.

Cycle stability of the electrodes was tested for 100 cycles, where no noticeable capacity fading was observed with high Coulombic efficiencies (Figure S9a and b). A long-lasting cyclability test was also conducted with the MFG sample at a current density of 1 A g^{-1}. Figure 5d shows that the MFG sample can be tested over 2,000 cycles without capacity degradation. Field-emission scanning electron microscopy (FE-SEM) and FT-IR analysis of the cycled electrodes indicated that there were no distinctive changes in morphology and surface functional groups such as C=O, which further supports superior cycle stability (Figure S10). Excellent cycle stability is thought to be related to stable covalent bonding of surface functional groups on the functionalized graphene nano-platelets and lithium storage without significant volume change, which is typically observed in intercalation-based cathodes.

Functionalized graphene nano-platelets may also exhibit a respectably high rate capability depending on the degree of functionalization. At a current rate of 2.0 A g^{-1}, HFG, MFG, and LFG delivered 175, 150, and 125 mAh g^{-1}, respectively. Even at 10 A g^{-1}, all the samples delivered ~100 mAh g^{-1}. The exceptional rate capability was attributed to the porous morphology of the functionalized graphene nano-platelets, allowing the electrolyte to easily penetrate into the pores, thus improving lithium ion transport from
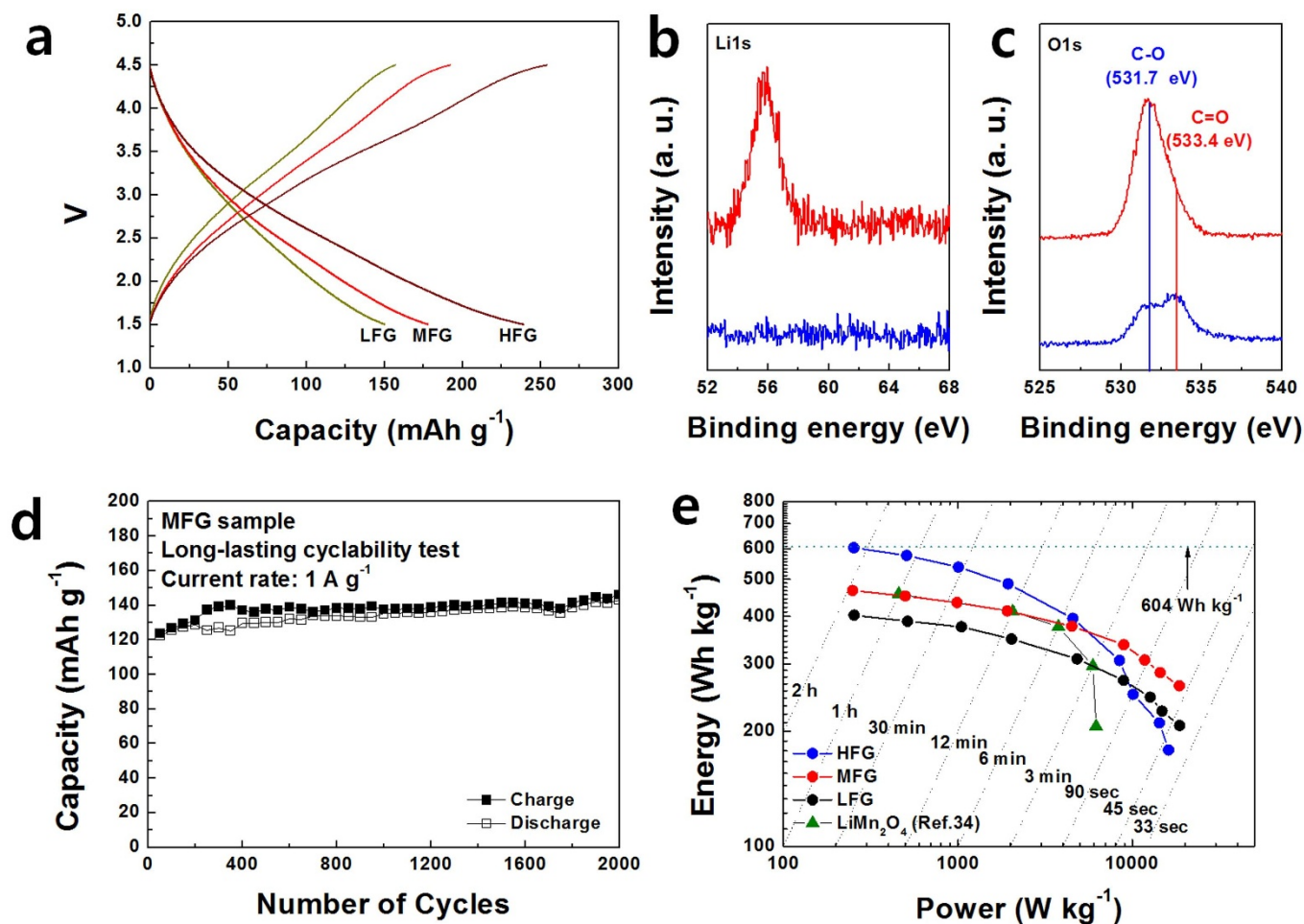
Figure 5 | Electrochemical performance of functionalized graphene nano-platelets with different degrees of oxidation (HFG, MFG, and LFG represent samples with high, medium, low contents of functional groups, respectively). (a) Charge/discharge profiles of the samples in which the profile shapes of the samples are similar to one another, demonstrating that the electrochemical reaction mechanism of each sample is similar. (b) *Ex-situ* XPS in Li1s region shows lithium ions are stored after discharge, (c) *Ex-situ* XPS in O1s region reveals that the C=O functional group becomes C–O after discharge process, indicating C=O functional group is the redox center for lithium storage. (d) Long-lasting cyclability test of the MFG sample at a high current rate of 1 Ag^{-1} up to 2,000 cycles. (e) Ragone plot for the functionalized graphene nano-platelet electrodes with different amounts of functional groups; a conventional electrode material, $LiMn_2O_4$, is shown for comparison. Only the functionalized graphene nano-platelet weight was considered in the gravimetric energy and power calculations.

the electrolyte to the functionalized graphene nano-platelets. It should be noted that, compared to the capacities delivered at a low current rate, higher rate performance was found in less oxidized samples (Figure S11). We believe that at high current densities, slight differences in the electrical conductivity of the samples led to substantial differences in rate performance. Figure S12 and Table S1 show that electrical conductivity increased with decreasing functional group content. The highest power performance was obtained from LFG, while the highest energy density was achieved with HFG. This indicates that power and energy density can be tuned simply by controlling the functional group content on graphene nano-platelets.

The dependence of power and energy density on functionalization is clearly shown in the Ragone plot of Figure 5e. The power capability of the functionalized graphene nano-platelets was reduced with an increasing degree of oxidation. Nevertheless, HFG still exhibited a very high gravimetric energy of ~250 Wh kg^{-1} at a gravimetric power over 10 kW kg^{-1} (at few minutes charge/discharge rate). The gravimetric energy of the functionalized graphene nano-platelets approached that of a commercially available high-power $LiMn_2O_4$ cathode. At current rates higher than 6 kW kg^{-1}, the functionalized graphene nano-platelets delivered significantly greater gravimetric energy (>1.5–1.8 times) than $LiMn_2O_4$ nanowires having the highest reported power capability[34].

Discussion

The high gravimetric energy and power were attributed to the fast surface Faradaic reaction between functional groups and lithium ions combined with the three-dimensional network framework of the functionalized graphene nano-platelets (Figure S13) and high electrical conductivity throughout the graphitic region (Figure S 13b). The lithium storage occurs at functional groups on the surface or at the edge of the graphene nano-platelets. It means that the delivery of lithium ions and electrons to the surface is likely the limiting factor for the electrochemical reaction similarly with Ref. 8. Therefore, it is important to form porous morphology to facilitate the accessibility of electrolyte to the electrode material. The suitable control of the electrode architecture by increasing active surface area with a stable interconnection of the electrode is expected to further increase the electrochemical performance of electrode materials based on C=O redox centers. In summary, functionalized graphene nano-platelets derived from a simple mass-scalable chemical method were found to be extremely promising as an electrode material for

rechargeable batteries that can deliver high gravimetric energies ($\sim$250 Wh kg^{-1}) at a power over 20 kW kg^{-1} for more than a thousand cycles. Moreover, we have demonstrated that gravimetric energy and power can be simply tuned by controlling the degree of oxidation, suggesting that further development of the electrode based on the same chemistry is possible. Low material cost and simple fabrication, combined with the tunable high power and energy density of this new class of cathodes, will open up new possibilities for the development of high-performance energy storage devices for various applications.

Method

Fabrication of functionalized graphene nano-platelets. Graphite oxide (GO) was initially fabricated by modifying the Hummers method[50]. NaNO$_3$ (1 g) and H$_2$SO$_4$ (45 mL) were added to graphite (1 g) and stirred for 30 min in an ice bath. Varying amounts (4–6 g) of an oxidizing agent, KMnO$_4$, were added to the resulting solution to control the degree of oxidation of the functionalized graphene nano-platelets, followed by stirring at 50°C for 2 h. Deionized (DI) water (100 mL) and H$_2$O$_2$ (6 mL, 35%) were slowly added to the solution and filtered with HCl (150 mL, 10%). Additional filtering with concentrated HCl (100 mL, 37%) was performed to retrieve the GO powder. Then, the samples were annealed at 120°C for 6 h. At this point, the color of the GO changed from dark brown to black, and the volume expanded significantly. It should be noted that functionalized graphene nano-platelets were not obtained below 120°C (Figure S14) and without concentrated HCl treatment. As a control, treatment was also carried out with NH$_3$ and H$_2$O instead of HCl. The degree of oxidation in the functionalized graphene nano-platelets was controlled by simply changing the amount of oxidizing agent from 4 g to 6 g and by additional heat treatment. The samples were labeled HFG, MFG, LFG, and MFG-400, representing samples with high, medium, and low contents of functional groups, while the MFG-400 sample underwent additional heat treatment at 400°C. All the samples were annealed at 120°C after HCl treatment to generate a porous morphology.

Characterization of functionalized graphene nano-platelets. The morphologies of graphite, GO, and functionalized graphene nano-platelets were investigated using field-emission scanning electron microscopy (FE-SEM, SUPRA 55VP) and high-resolution transmission electron microscopy (HR-TEM, JEM-3000F). The structures were analyzed with an X-ray diffractometer (XRD, D8-Advance) using Cu Kα radiation over a scan range of 5–45° and Fourier transform infrared (FT-IR, Hyperion 3000) spectroscopy. X-ray photoelectron spectroscopy (XPS, AXIS-HSi) and an element analyzer (EA, EA11110-FISONS and FlashEA 1112) were used to determine the degree of oxidation of GO and the amount of functional groups in functionalized graphene nano-platelets. Ex-situ and in-situ mass spectrometry (MS, HPR-20, Hiden Analytical) were used to understand the effect of HCl on pore formation and the reduction of GO. The electrical conductivities of the functionalized graphene nano-platelets with different degrees of oxidation were measured using a four-point probe method for pelletized powder.

Electrochemical characterization. Electrodes were prepared by mixing the active material (functionalized graphene nano-platelets with different degrees of oxidation, 72 wt%) with polyvinylidene fluoride binder (18 wt%) and super-P (10 wt%) in an N-methyl-2-pyrrolidone solvent. The resulting slurry was uniformly pasted onto Al foil, dried at 120°C for 2 h, and roll-pressed. Test cells were assembled in a two-electrode configuration with a Li metal counter electrode, a separator (Celgard 2400), and an electrolyte of 1 M lithium hexafluorophosphate in a 1 : 1 mixture of ethylene carbonate and dimethyl carbonate (Techno Semichem) in a glove box. The loading density of the electrodes was 1.4–1.6 g cm^{-2}. Electrochemical profiles were obtained over a voltage range from 4.5 to 1.5 V at varying current rates from 0.1 to 10.0 A g^{-1} using a multichannel potentio-galvanostat (WonATech). Cyclic voltammetry (CV) measurements were performed using the same cell configuration with potentiao-galvanostat tests in the voltage range from 4.5 to 1.5 V at a scan rate of 0.1 mV sec^{-1}. The capacitance values were calculated from the CV curves by dividing the current by the voltage scan rate.

1. Yang, Z. et al. Electrochemical energy storage for green grid. Chem. Rev. 111, 3577–3613 (2011).
2. Gaines, L. & Cuenca, R. Report#ANL/ESD-42. Argonne National Laboratory May (2000).
3. Whittingham, M. S. Lithium batteries and cathodes materials. Chem. Rev. 104, 4271–4301 (2004).
4. Howard, W. F. & Spontnitz, R. M. Theoretical evaluation of high-energy lithium metal phosphate cathode materials in Li0ion batteries. J. Power Sources 165, 887–891 (2007).
5. Meethong, N., Shadow, H.-Y., Speakman, S. A., Carter, W. C. & Chiang, Y.-M. Strain accommodation during phase transformations in olivine-based cathodes as a materials selection criterion for high-power rechargeable batteries. Adv. Funct. Mater. 17, 1115–1123 (2007).
6. Ellis, B. L., Makahnouk, W. R. M., Makimura, Y., Toghill, K. & Nazar, L. F. A multifunctional 3.5 V iron-based phosphate cathode for rechargeable batteries. Nat. Mater. 6, 749–753 (2007).
7. Bruce, P. G., Armstrong, A. R. & Gitzendanner, R. L. New intercalation compounds for lithium batteries: layered LiMnO$_2$. J. Mater. Chem. 9, 193–198 (1999).
8. Kang, B. & Ceder, G. Battery materials for ultrafast charging and discharging. Nature 458, 190–193 (2009).
9. Arico, A. S., Bruce, P., Scrosati, B., Tarascon, J.-M. & Schalkwijk, W. V. Nanostructured materials for advanced energy conversion and storage devices. Nat. Mater. 4, 366–377 (2005).
10. Armand, M. & Tarascon, J.-M. Building better batteries. Nature 451, 652–657 (2008).
11. Chan, C. K. et al. High-performance lithium battery anodes using silicon nanowires. Nat. Nanotech. 3, 31–35 (2008).
12. Kim, M. G. & Cho, J. Reversible and high-capacity nanostructured electrode materials for Li-ion batteries. Adv. Funct. Mater. 19, 1497–1514 (2009).
13. Cheng, F., Tao, Z., Liang, J. & Chen, J. Template-directed materials for rechargeable lithium-ion batteries. Chem. Mater. 20, 667–681 (2008).
14. Kim, S.-W. et al. Fabrication and electrochemical characterization of TiO$_2$ three-dimensional nanonetwork based on peptide assembly. ACS Nano 3, 1085–1090 (2009).
15. Lee, Y. J. et al. Fabricating genetically engineered high-power lithium-ion batteries using multiple virus genes. Science 324, 1051–1055 (2009).
16. Kim, H. et al. Nano-graphite platelet loaded with LiFePO$_4$ nanoparticles used as the cathode in a high performance Li-ion battery. Carbon 50, 1966–1971 (2012).
17. Wang, H. et al. LiMn$_{1-x}$Fe$_x$PO$_4$ nanorods grown on graphene sheets for ultrahigh-rate-performance lithium ion batteries. Angew. Chem. 123, 7502–7506 (2011).
18. Zhou, Y., Wang, J., Hu, Y., O'Hayre, R. & Shao, Z. A porous LiFePO$_4$ and carbon nanotube composite. Chem. Commun. 46, 7151–7153 (2010).
19. Kim, S.-W., Seo, D.-H., Gwon, H., Kim, J. & Kang, K. A porous LiFePO$_4$ and carbon nanotube composite. Adv. Mater. 22, 5260–5264 (2010).
20. Sathiya, M., Prakash, A. S., Ramesha, K., Tarascon, J.-M. & Shukla, A. K. V$_2$O$_5$-anchored carbon nanotubes for enhanced electrochemical energy storage. J. Am. Chem. Soc. 133, 16291–16299 (2011).
21. Ding, K. et al. Preparation of nano-structured LiFePO$_4$/graphene composites by co-precipitation method. Electrochem. Commun. 12, 10–13 (2010).
22. Bak, S.-M. et al. Spinel LiMn$_2$O$_4$/reduced graphene oxide hybrid for high rate lithium ion batteries. J. Mater. Chem. 21, 17309–17315 (2011).
23. Zhou, X., Wang, F., Zhu, Y. & Liu, Z. Graphene modified LiFePO$_4$ cathode materials for high power lithium ion batteries. J. Mater. Chem. 21, 3353–3358 (2011).
24. Sun, Y., Wu, Q. & Shi, G. Graphene based new energy materials. Energy Enviorn. Sci. 4, 1113–1132 (2011).
25. Gwon, H. et al. Flexible energy storage devices based on graphene paper. Energy Environ. Sci. 4, 1277–1283 (2011).
26. Simon, P. & Gogotsi, Y. Materials for electrochemical capacitors. Nat. Mater. 7, 845–854 (2008).
27. Oda, H., Yamashita, A., Minoura, S., Okamoto, M. & Morimoto, T. Modification of the oxygen-containing functional group on activated carbon fiber in electrodes of an electric double-layer capacitor. J. Power Sources 158, 1510–1516 (2006).
28. Fan, X., Lu, Y., Xu, H., Kong, X. & Wang, J. Reversible redox reaction on the oxygen-containing functional groups of an electrochemically modified graphite electrode for the pseudo-capacitance. J. Mater. Chem. 21, 18753–18760 (2011).
29. Lee, S. W. et al. High-power lithium batteries from functionalized carbon-nanotube electrodes. Nat. Nanotech. 5, 531–537 (2010).
30. Lee, S. W., Gallant, B. M., Byon, H. R., Hammond, P. T. & Shao-Horn, Y. Nanostructured carbon-based electrodes: bridging the gap between thin-film lithium-ion batteries and electrochemical capacitors. Energy Environ. Sci. 4, 1972–1985 (2011).
31. Lee, S. W. et al. Self-standing positive electrodes of oxidized few-walled carbon nanotubes for light-weight and high-power lithium batteries. Energy Environ. Sci. 5, 5437–5444 (2012).
32. Yoo, E. et al. Large reversible Li storage of graphene nanosheet families for use in rechargeable lithium ion batteries. Nano Lett. 8, 2277–2282 (2008).
33. Reddy, A. L. M. et al. Synthesis of nitrogen-doped graphene films for lithium battery application. ACS Nano 4, 6337–6342 (2010).
34. Lee, H.-W. et al. Ultrathin spinel LiMn$_2$O$_4$ nanowires as high power cathode materials for Li-ion batteries. Nano Lett. 10, 3852–3856 (2010).
35. Perry, R. H. & Green, D. W. Perry's chemical engineers' handbook, 7th ed., New York, McGraw-Hill. (1997).
36. Dikin, D. A. et al. Preparation and characterization of grahene oxide paper. Nature 448, 457–460 (2007).
37. Park, S. et al. Aqueous suspension and characterization of chemically modified graphene sheets. Chem. Mater. 20, 6592–6594 (2008).
38. Park, S. et al. Colloidal suspensions of highly reduced graphene oxide in a wide variety of organic solvents. Nano Lett. 9, 1593–1597 (2009).
39. Yuan, Y. F., Xia, X. H., Yang, J. L., Chen, Y. B. & Guo, S. Y. Hierarchically ordered porous nickel oxide array film with enhanced electrochemical properties for lithium ion batteries. Electrochem. Commun. 12, 890–893 (2010).

40. Demir-Cakan, R., Hu, Y.-S., Antonietti, M., Maier, J. & Titirici, M.-M. Facile one-pot synthesis of mesoporous SnO_2 microspheres via nanoparticles assembly and lithium storage properties. *Chem. Mater.* **20**, 1227–1229 (2008).

41. Kim, H. *et al.* Graphene-based hybrid electrode material for high-power lithium-ion batteries. *J. Electrochem. Soc.* **158**, A930–A935 (2011).

42. Stanokovich, S. *et al.* Synthesis of graphene-based nano-plateletss via chemical reduction of exfoliated graphite oxide. *Carbon* **45**, 1558–1565 (2007).

43. Dreyer, D. R., Park, S., Bielawski, C. W. & Ruoff, R. S. The chemistry of graphene oxide. *Chem. Soc. Rev.* **39**, 228–240 (2010).

44. Park, S. *et al.* Chemical structures of hydrazine-treated graphene oxide and generation of aromatic nitrogen doping. *Nat. Commun.* **3**, 638 (2012).

45. Zhu, Y. *et al.* Exfoliation of graphite oxide in propylene carbonate and thermal reduction of the resulting graphene oxide platelets. *ACS Nano* **4**, 1227–1233 (2010).

46. Lu, G., Ocola, L. E. & Chen, J. Reduced graphene oxide for room-temperature gas sensors. *Nanotechnology* **20**, 445502 (2009).

47. Chen, H. *et al.* From biomass to a renewable $Li_xC_6O_6$ organic electrode for sustainable Li-ion batteries. *ChemSusChem* **1**, 348–355 (2008).

48. Han, X., Chang, C., Yuan, L., Sun, T. & Sun, J. Aromatic carbonyl derivative polymers as high-performance Li-ion storage materials. *Adv. Mater.* **19**, 1616–1621 (2007).

49. Gall, T. L., Reiman, K. H., Grossel, M. C. & Owen, J. R. Poly(2,5-dihydroxy-1,4-benzoquinon-3,6-methylene): a new organic polymer as positive electrode material for rechargeable lithium batteries. *J. Power Sources* **119–121**, 316–320 (2003).

50. Hummers, W. S. & Offeman, R. E. Preparation of graphitic oxide. *J. Am. Chem. Soc.* **80**, 1339 (1958).

Author contributions

H.K. and K.K. designed the experiments. H.K., H.D.L. and S.W.K. performed the experiments. H.K., H.D.L., S.W.K., J.H., D.H.S. and D.C.K. prepared the samples and analyzed the data. S.J., S.P. and K.K. participated in interpreting and analyzing the data. S.J., S.P. and K.K. reviewed and commented on the manuscript. H.K. wrote the manuscript. All authors discussed the results and commented on the manuscript.

Additional information

Supplementary information accompanies this paper at http://www.nature.com/scientificreports

How to cite this article: Kim, H. *et al.* Scalable Functionalized Graphene Nano-platelets as Tunable Cathodes for High-performance Lithium Rechargeable Batteries. *Sci. Rep.* **3**, 1506; DOI:10.1038/srep01506 (2013).